Electronic Supplementary Material (ESI) for Physical Chemistry Chemical Physics
This journal is © the Owner Societies 2015

**Electronic Supplementary Information**

# Ligand-exchange mechanism: new insight into solid-phase extraction of uranium based on a combined experimental and theoretical study

Yin Tian,[a,b] Jia Fu,[b] Yi Zhang,[b] Kecheng Cao,[a] Chiyao Bai,[a] Dongqi Wang,[d] Shoujian Li,*[,a] Ying Xue,*[,a] Lijian Ma,*[,a] Chong Zheng*[,c]

[a] *College of Chemistry, Sichuan University, Chengdu 610064, People's Republic of China*

[b] *College of Physical Science and Technology, Sichuan University, Chengdu 610064, People's Republic of China*

[c] *Department of Chemistry and Biochemistry, Northern Illinois University, DeKalb, Illinois 60115, USA*

[d] *CAS Key Laboratory of Nuclear Radiation and Nuclear Energy Techniques, and Institute of High Energy Physics, Chinese Academy of Sciences, Beijing 100049, China*

Corresponding authors: sjli000616@scu.edu.cn; yxue@scu.edu.cn; ma.Lj@163.com; cz1212@yahoo.com

# 1. Synthesis and characterization of solid-phase extractant: Urea-functionalized graphite oxide (Urea-GO)

## 1.1 Preparation of graphite oxide (GO)

GO was synthesized from natural graphite powder using Hummers method.[1] At first, 10g of graphite powder was added to 230mL of concentrated $H_2SO_4$. Then, about 30g of $KMnO_4$ was added gradually with stirring in an ice bath. The temperature of the suspension was maintained below 10 °C. After removal of the ice-bath, the suspension was stirred at room temperature for 30 min. Then distilled water (230 mL) was slowly added to cause an increase in temperature to 98 °C and the suspension was maintained at that temperature for 15 min. And then 100 mL of $H_2O_2$ was added to the system before further dilution with plenty of distilled water (1.4 L). The solid product was separated by centrifugation, and washed repeatedly with 5% HCl solution until sulphate could not be detected with $BaCl_2$, then washed with distilled water until the pH of the washes becomes neutral and finally dried at 55 °C in vacuum.

## 1.2 Scanning electron microscope SEM

The morphologies of GO and its derivatives were studied using SEM as shown in Figure S1. The pattern of GO shows a lamellar structure with a number of smooth sheets stacking together (Figure S1a). While for di-isocyanate-functionalized graphite oxide (iGO) and Urea-GO, the surface-covering sheets and the edges of sheets

gradually became rougher and thicker respectively after grafting with TDI (Figure S1b) and subsequently modifying with ETA (Figure S1c).

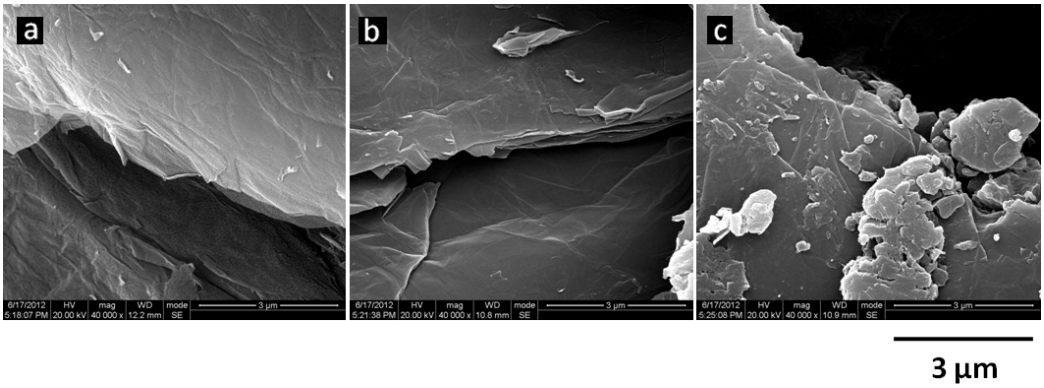


**Figure S1. SEM images of (a) GO, (b) iGO, (c) Urea-GO**

### 1.3 Fourier transform infrared (FT-IR) spectra

For FT-IR characterization, the test sample is prepared according to following procedure: firstly, transfer some KBr out of an oven (at a constant temperature of 100°C) into a mortar, add about 1 to 2 % of the GO-based solid sample, mix and grind to a fine powder, then, the powder is tabletted using an infrared manual press to obtain the FT-IR pellet.

FT-IR spectra of GO, iGO and Urea-GO are shown in Figure S2. Figure S2a represents a typical FTIR spectrum of GO. The absorption band at 1728 $cm^{-1}$ is attributed to the stretching vibration of the C=O bond of carboxyl groups. The stretching vibration of C–O–C and C–OH functional groups is observed at 1053 $cm^{-1}$ and 1224 $cm^{-1}$, respectively. The band at 1617 $cm^{-1}$ is assigned to the deformation vibrations of the adsorbed water molecules or the free hydroxyl groups.[2–4]

As shown in Figure S2b, after grafting TDI onto GO, the new band at 2274 $cm^{-1}$ is attributed to the stretch of –NCO groups. The new band at 1643 $cm^{-1}$ is attributed to an amide carbonyl-stretching mode, and the band at 1542 $cm^{-1}$ can originate from carbamate esters and corresponds to the coupling of the C–N stretching vibration with the CHN deformation vibration. The bands at 1597 $cm^{-1}$ and 1448 $cm^{-1}$ can be assigned to benzene ring skeleton vibration. So it could be conjectured that the –NCO groups of TDI are chemically grafted on GO sheets through carbamate esters linkage.[2,5]

For Urea-GO (Figure S2c), after modification with ethanolamine, the –NCO absorption band at 2274 $cm^{-1}$ disappears. The band at 1641 $cm^{-1}$ can be assigned to NH–CO in urea and carbamate, and furthermore, the other absorption bands in Figure 2b retain unchanged which conforms the occurrence of chemical reaction between the –NCO groups on iGO and the $–NH_2$ groups of ETA. The data suggest that the desired modification has been achieved. We must point out that the isocyanate groups react with amines much faster than alcohols.[6]

The sample preparation process for FT-IR characterization: Firstly, the small amount of solid material was mixed with potassium bromide (KBr, SP). And then, the test sample was obtained by grinding and pressing.

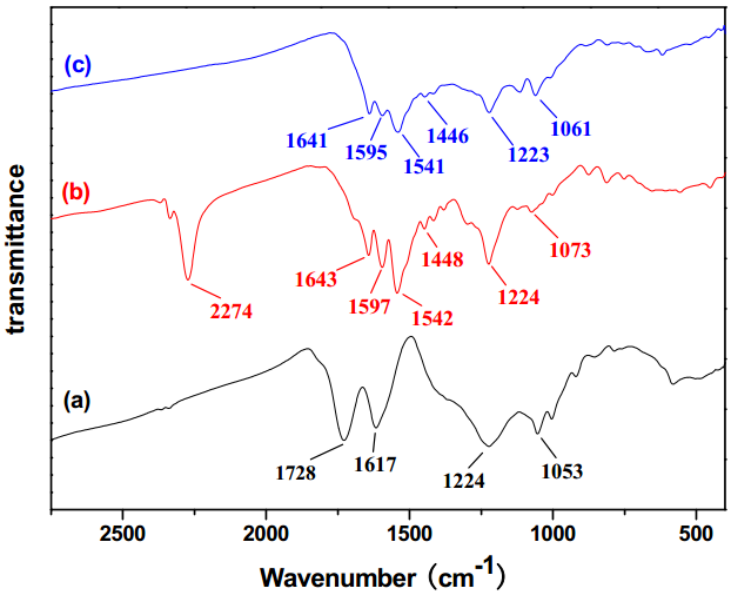


**Figure S2. FT-IR spectra of (a) GO, (b) iGO, (c) Urea-GO**

### 1.4 X-ray photoelectron spectroscopy (XPS) measurements

The GO, Urea-GO and Urea-GO-U samples were characterized by XPS in Figure S3 (a). We can find three peeks, C 1S: 284–286 eV, N 1S: 399.4–401.7 eV, O 1S: 531.5–533.5 eV, U 4f: 375–400 eV. It is observed that content of nitrogen was increased obviously after chemical modification, and the content of uranium was appeared obviously after extraction experiments. The C1s XPS spectrum of GO (Figure S3b) showed binding energies at 284.6 eV (C–C and C–H) , 286.6 eV ( C–OH and C–O–C), 288.3 eV (O–C=O). In Figure S3c, The peak at 288.1 eV was attributed

to amide (N−C=O), and the peak at 289.2 eV to urea structure, both corresponded to grafting of TDI and ETA.[7−9]

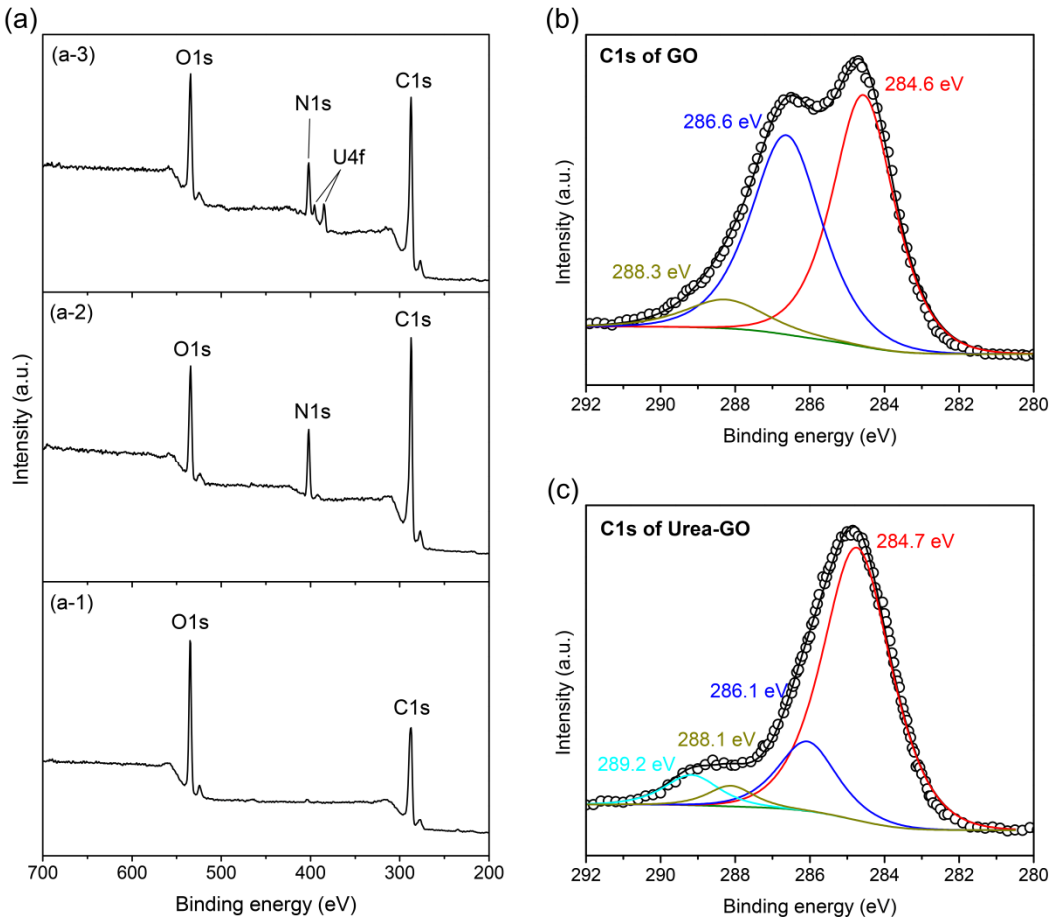


**Figure S3. The X-ray photoelectron spectroscopy.** (a) XPS survey spectra of (a-1) GO, (a-2) Urea-GO, (a-3) Urea-GO-U. (b) C 1s core-level spectra of GO is fitted with Gaussian-Lorentzian waveforms. (c) C 1s core-level spectra of Urea-GO is fitted with Gaussian-Lorentzian waveforms.

### 1.5 The X-ray diffraction (XRD)

Figure S4 shows the X-ray diffraction patterns of the pristine graphite (PG), GO and Urea-GO. The PG shows a strong peak at 2θ = 26.60°, which indicates that the average interlayer spacing of PG is 3.35 Å. But after chemical modification, the characteristic 2θ peak of GO appearing at 10.10° corresponds to an average interlayer spacing of 8.76Å. Compared to GO, the diffraction peak of the Urea-GO shifts toward to a lower 2θ angle of 7.94° and, therewith, the interlayer spacing is increased to 11.13 Å due to presence of the urea groups between the sheets of the GO. This result

provides further support for the in situ assembly of the urea moieties to the interlayer and surface of the GO sheets.[5]

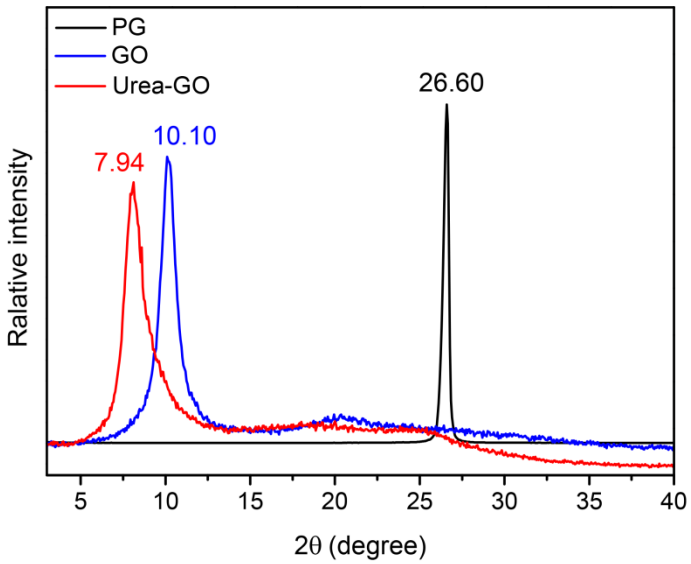


**Figure S4. The X-ray diffraction (XRD).** XRD pattern of pristine graphite (PG), GO and Urea-GO.

### 1.6 Elemental analysis (EA)

Table S1 collects the results of the elemental analysis of the samples. An obvious increase in N% from GO to iGO corresponds to the loading of TDI onto GO matrix. About 2.79 mmol TDI per gram of iGO are calculated from the increment of N content. From iGO to Urea-GO, the content of nitrogen continues to increase, which suggests that ETA has been assembled successfully on iGO sheets as shown in Figure 1. The loading ratio of ETA could be calculated as 0.578 mmol $g^{-1}$ on Urea-GO. The results are in agreement with the outcome of the FTIR spectra.

**Table S1. Elemental analysis of GO and its derivatives**

| Simple | C% | H% | N% |
|---|---|---|---|
| GO | 50.70 | 2.21 | 0.00 |
| iGO | 58.50 | 3.15 | 7.84 |
| Urea-GO | 57.40 | 3.97 | 8.37 |

## 2. The hydration sphere of uranyl ions and density functional theory (DFT) calculations.

A clear understanding of uranyl speciation at high nitrate concentration solution is very important because there are generally numerous nitrate ions in real nuclear industry effluents.[10,11] The crystal structure of $UO_2(NO_3)_2(H_2O)_2$ reveals that the two nitrates bind in a bidentate mode in the equatorial plane of the uranyl ions,[12,13] and, on the other hand, theoretical research also demonstrated that the uranyl species also prefers this binding motif in nitrate solution.[14]

Therefore, the most practical solvation model should comprise the explicit inclusion of waters in the first solvation sphere combined with continuum solvation model for the remainder of the solvation sphere.[15] Now, uranyl pentahydrate $[UO_2(H_2O)_5]^{2+}$ and uranyl nitrate dihydrate $UO_2(NO_3)_2(H_2O)_2$ structures were optimized at the B3LYP/6-31G(d)/RECP level of theory in gas phase (298.15 K, 0.1 MPa) and in aqueous solution (CPCM, UFF). The optimized structures of $[UO_2(H_2O)_5]^{2+}$ and $UO_2(NO_3)_2(H_2O)_2$ are shown in Figure S5. These results along with other available experimental and theory data were shown in Table S4 and Table S5 for comparison. To provide insight into the bonding nature of these species, NBO analysis was performed at the same level of theory (Table S3). As reported in Table S4 and Table S5, All optimized geometrical parameters agree well with both experimental and theoretical data.

For the interaction between the uranyl hydrates ($[UO_2(H_2O)_5]^{2+}$) and nitrate ions in the same adsorption system, the changes in enthalpy and the Gibbs free energy are −169.84 and −184.97 kJ $mol^{-1}$ (see Table S2), respectively, suggesting that the neutral uranyl nitrate hydrates ($UO_2(NO_3)_2(H_2O)_2$) is more stable than the charged uranyl hydrate $[UO_2(H_2O)_5]^{2+}$. That is, nitrate ion, which acts as bidentate ligand in this case, has much stronger coordination ability towards uranyl than water molecule. Therefore, uranyl ion prefers to coordinate to the nitrate ion when nitrate ions exist in aqueous reaction medium.[16]

Meanwhile, for uranyl nitrate hydrates ($UO_2(NO_3)_2(H_2O)_2$), Shi et al.[16] report only one conformer like (1) in Figure S5(e), and other researcher don't pay great attention to the conformers of $UO_2(NO_3)_2(H_2O)_2$. But we found that $UO_2(NO_3)_2(H_2O)_2$ exists in two different conformations, which are shown in Figure S5(e). The $\Delta H$, $\Delta S$ and $\Delta G$ of

the (1)→(2) process in aqueous medium (in Table S2) indicate that this process is a spontaneous exothermic process and (2) is the lower energy conformer. So, (2) is more stability conformer.

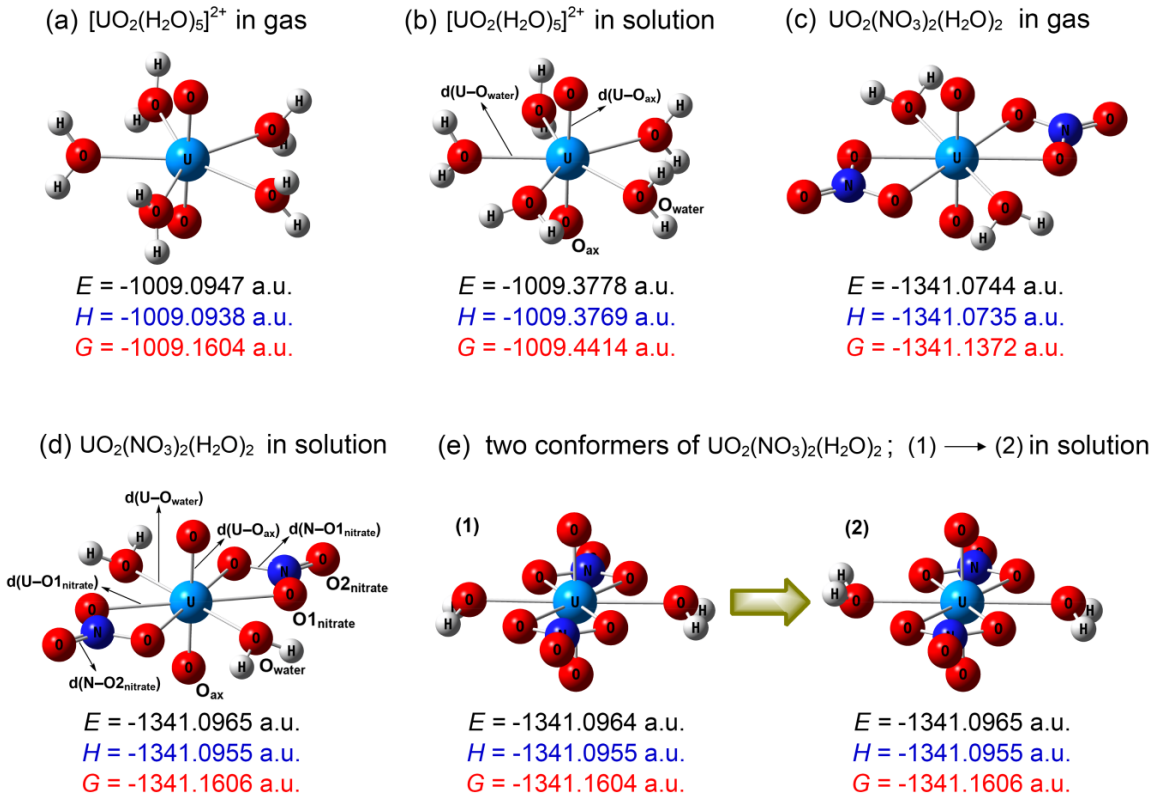


**Figure S5. The structure of uranyl ion in gas (298.15 K, 0.1 MPa) and in aqueous solution(CPCM).** The optimized structures of the stationary points for uranyl hydrates ($[UO_2(H_2O)_5]^{2+}$) (a) in gas and (b) in aqueous solution obtained by the DFT calculations. (b) The optimized structures of the stationary points for uranyl nitrate hydrates ($UO_2(NO_3)_2(H_2O)_2$) (c) in gas and (d) in aqueous solution obtained by the DFT calculations. (e) The optimized structures of two conformers for $UO_2(NO_3)_2(H_2O)_2$ obtained by the DFT calculations.

**Table S2. The changes in enthalpy (Δ*H*, kJ mol$^{-1}$), entropy (Δ*S*, J mol$^{-1}$ K$^{-1}$), and gibbs free energy (Δ*G*, kJ mol$^{-1}$) for the process (a) →(b) and (1)→(2) in aqueous solution (CPCM, UFF) at Figure S5.**

| reaction | Δ*H* | Δ*S* | Δ*G* |
|---|---|---|---|
| $[UO_2(H_2O)_5]^{2+} + 2(NO_3)^- \rightarrow [UO_2(NO_3)_2(H_2O)_2] + 3H_2O$ | −169.84 | 50.77 | −184.97 |
| (1)→(2) | −0.01 | 1.08 | −0.42 |

**Table S3. The NBO analysis of uranyl hydrates ($[UO_2(H_2O)_5]^{2+}$) and uranyl nitrate hydrates ($UO_2(NO_3)_2(H_2O)_2$).** The wiberg bond orders (WBOs) of U–O bonds and nature charges on uranium and oxygen atom in the aqueous solution (CPCM).

| species | $U–O_{ax}$ | $U–O_{water}$ | $U–O1_{nitrate}$ | Q(U) | $Q(O_{ax})$ | $Q(O_{water})$ | $Q(O1_{nitrate})$ |
|---|---|---|---|---|---|---|---|
| $[UO_2(H_2O)_5]^{2+}$ | 2.210 | 0.433 | – | 1.802 | −0.501 | −0.876 | – |
| $UO_2(NO_3)_2(H_2O)_2$ | 2.178 | 0.410 | 0.461 | 1.477 | −0.526 | −0.860 | −0.443 |

**Table S4. The selected geometrical parameters of $[UO_2(H_2O)_5]^{2+}$ obtained by the DFT calculations in comparison with available experimental and theory data.** The average bond lengths (Å) $d(U–O_{ax})$, $d(U–O_{water})$ are described in Figure S6(a). The $\theta(O_{ax}–U–O_{ax})$ denote the bond angle (degree) and the $n(H_2O)_{eq}$ refers to the hydration number in the first solvation sphere (in the equatorial plane).

| | | $d(U–O_{ax})$ | $d(U–O_{water})$ | $\theta(O_{ax}–U–O_{ax})$ | $n(H_2O)_{eq}$ |
|---|---|---|---|---|---|
| Theory | This work (in gas) | 1.747 | 2.484 | 179.73 | 5 |
| | This work (in solution) | 1.755 | 2.463 | 178.34 | 5 |
| | VASP (GGA) [17] | 1.82 | 2.43 | 174 | 5 |
| | Hartree-Fock [18] | 1.70 | 2.50 | | 5 |
| | DFT (PBE96) [19] | 1.77 | 2.44 | 179.8 | 5 |
| | DFT (B3LYP) [20] | 1.787 | 2.424 | | 5 |
| | DFT (B3LYP) [21] | 1.756 | 2.516 | | 5 |
| | DFT (SVWN) [21] | 1.778 | 2.423 | | 5 |
| experiment | HEXS [22] | 1.766 | 2.420 | | 5 |
| | EXAFS [23] | 1.76 | 2.41 | | 4.7 |
| | EXAFS [24] | 1.76 | 2.41 | | 5.3 |
| | EXAFS [25] | 1.78 | 2.41 | | 4.5±0.4 |
| | XRD [26] | 1.702 | 2.421 | | 5 |
| | XRS [27] | 1.766 | 2.420 | | 4/5 |
| | EXAFS [28] | 1.77 | 2.42 | | 4.7 |

**Table S5. The selected geometrical parameters of $UO_2(NO_3)_2(H_2O)_2$ obtained by the DFT calculations in comparison with available experimental and theory data.** The average bond lengths (Å) $d(U–O_{ax})$, $d(U–O_{water})$, $d(U–O1_{nitrate})$, $d(N–O2_{nitrate})$ and $d(N–O1_{nitrate})$ are described in Figure S6(b).

| | | $d(U–O_{ax})$ | $d(U–O_{water})$ | $d(U–O1_{nitrate})$ | $d(N–O2_{nitrate})$ | $d(N–O1_{nitrate})$ |
|---|---|---|---|---|---|---|
| theory | This work (in gas) | 1.766 | 2.541 | 2.473 | 1.204 | 1.289 |
| | This work (in solution) | 1.768 | 2.521 | 2.486 | 1.209 | 1.285 |
| | Hartree-Fock[29] | 1.72 | 2.49 | | 1.20 | 1.31 |
| experiment | Neutron Diffraction[12] | 1.76 | 2.40 | 2.53 | | |
| | Neutron Diffraction[13] | 1.758 | 2.452 | 2.497 | 1.202 | 1.265 |
| | XRD[30] | 1.75 | 2.39 | 2.53 | 1.22 | 1.27 |

## 3. Density functional theory (DFT) calculations are used to explore coordinating atoms

the coordination ability of three possible coordinating atoms on Urea-GO, including the hydroxylic oxygen atom, the double bond oxygen in urea and nitrogen atom in urea, with uranyl hydrates ($[UO_2(H_2O)_5]^{2+}$) in aqueous solution were evaluated by DFT calculations (reaction: $[UO_2(H_2O)_5]^{2+} + L \rightarrow [UO_2L(H_2O)_{5-x}]^{2+} + xH_2O$, x=1 for oxygen and x=2 for nitrogen). The coordination structures are described in Figure S6. The Wiberg bond orders (WBOs) and selected natural charges (Q) and changes in atom charges (ΔQ) in aqueous solution obtained by natural bond orbital (NBO) analysis are listed in Table S6.

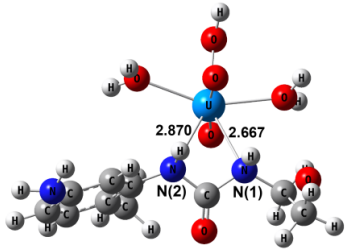


**(a-1) nitrogen**

*E* = -1561.1049 a.u.
*H* = -1561.1040 a.u.
*G* = -1561.1905 a.u.

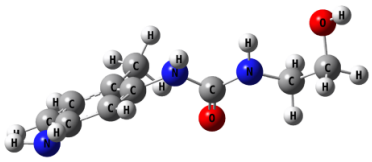

**(a-2) urea conformer-1**

*E* = -704.5492 a.u.
*H* = -704.5483 a.u.
*G* = -704.6087 a.u.

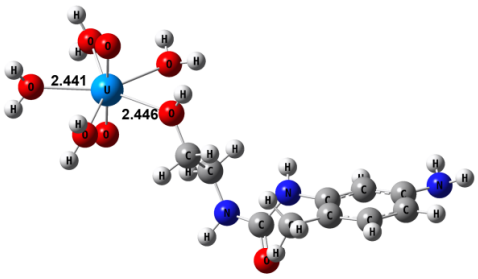


**(b-1) hydroxyl oxygen**

*E* = -1637.5275 a.u.
*H* = -1637.5265 a.u.
*G* = -1637.6230 a.u.

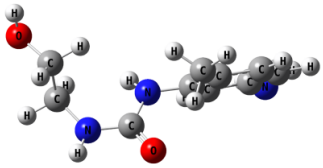

**(b-2) urea conformer-2**

*E* = -704.5446 a.u.
*H* = -704.5436 a.u.
*G* = -704.6046 a.u.

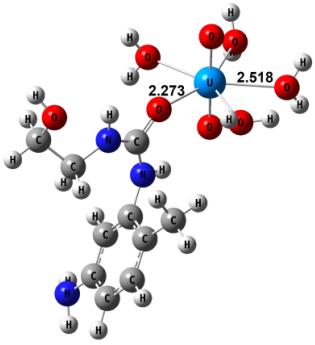


**(c-1) ketone oxygen**

*E* = -1637.5473 a.u.
*H* = -1637.5463 a.u.
*G* = -1637.6426 a.u.

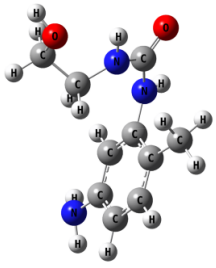

**(c-2) urea conformer-3**

*E* = -704.5405 a.u.
*H* = -704.5396 a.u.
*G* = -704.6002 a.u.

**Figure S6. Searching for coordinating atom.** The optimized coordinating structures of the uranyl with different coordinating atom in urea including (a-1) the nitrogen atom, (b-1) the hydroxylic oxygen atom and (c-1) the double bond oxygen which corresponds to three optimized urea conformers of the stationary points (a-2), (b-2) and (c-2). The important bond lengths for the extraction structures are also depicted.

**Table S6. The NBO analysis of coordination structures in Figure S7.** The Wiberg bond orders (WBOs) of chemical bonds between uranium and coordinating atom (U–(CA)), selected natural charges (Q) and changes in atom charges (ΔQ) in the aqueous solution (CPCM, UFF) obtained by the B3LYP method

| coordinating atom | Q(CA) | ΔQ (CA) | ΔQ (U) | U–(CA) |
|---|---|---|---|---|
| nitrogen N1 | −0.690 | −0.034 | 0.079 | 0.340 |
| nitrogen N2 | −0.689 | 0.014 | | 0.248 |
| hydroxyl oxygen | −0.777 | 0.065 | −0.008 | 0.442 |
| ketone oxygen | −0.725 | 0.070 | −0.098 | 0.699 |

**Table S7. The steric-hindrance effect of ligand.** The changes in enthalpy (Δ*H*, kJ $mol^{-1}$), entropy (Δ*S*, J $mol^{-1}$ $K^{-1}$), and gibbs free energy (Δ*G*, kJ $mol^{-1}$) for the change in structures of urea from three stable conformers to coordinated structure of them in aqueous solution (CPCM, UFF) at Figure S6.

| urea structure | Δ*H* | Δ*S* | Δ*G* |
|---|---|---|---|
| comformer-1 (a-2) → coordinated structure in (a-1) | 32.96 | −14.53 | 37.29 |
| comformer-2 (b-2) → coordinated structure in (b-1) | 3.63 | −11.54 | 7.07 |
| comformer-3 (c-2) → coordinated structure in (b-1) | 15.21 | −20.28 | 21.25 |

## 4. DFT calculations is used to investigate the mechanism of extraction

The alkyl phosphate ester (APE), such as tri-n-butyl phosphate (TBP), n-octyl(phenyl)-N, N-diisobutyl-methylcarbamoyl phosphine oxide (CMPO), were mostly employed in uranium LLE process at industrial scale (for example PUREX process and so on).[31] We investigated the interaction processes of the urea ligand on the as-synthesized solid-phase extractant with uranyl ion using DFT calculations, along with the trimethyl phosphate (TMP, which is similar to TBP, used for simplifying the calculation)[32,33] for comparison.

### 4.1 Extraction reaction processes

The optimized structures of reactant complexes (RC), transition states (TS) and product complexes (PC) for urea/TMP extraction processes in aqueous solution are shown in Figure S7 (Figure S9 in gas). Meanwhile, the potential energy profiles for the reactions in aqueous solution are presented in Figure S8 (Figure S10 in gas), and the changes in enthalpy($\Delta H$), Entropy($\Delta S$) and Gibbs free energy ($\Delta G$) in aqueous solution are given in Table S7 (Table 11 in gas). It can be observed that both ligand-water exchanges are exothermic process. The activation energy barrier of the urea-involving process is 35.75 kJ/mol, lower than that in TMP-involving process (40.09 kJ/mol), which indicates that the ligand-water interchange mechanism may be slightly more favorable for urea-involving process than for TMP-involving process. And the lower activation barrier will be induced by the more negative $\Delta$q values, defined as q(atom in TS) – q (atom in RC),[34] shown in Table S10. In the transition state (TS) for extraction reactions of urea and TMP ligands, Urea-TS and TMP-TS, the imaginary frequency are 66.81i $cm^{-1}$ and 29.68i $cm^{-1}$ ( −56.99i $cm^{-1}$ and −68.69i $cm^{-1}$ in gas), respectively, associated with the nucleophilic attack of the $O_L$ atom to the U atom. Our calculations figure out that uranyl extraction processes of urea and TMP have nearly similar minimal energy path, indicating that the urea structure has nearly the same strong uranyl extraction ability as alkyl phosphates.

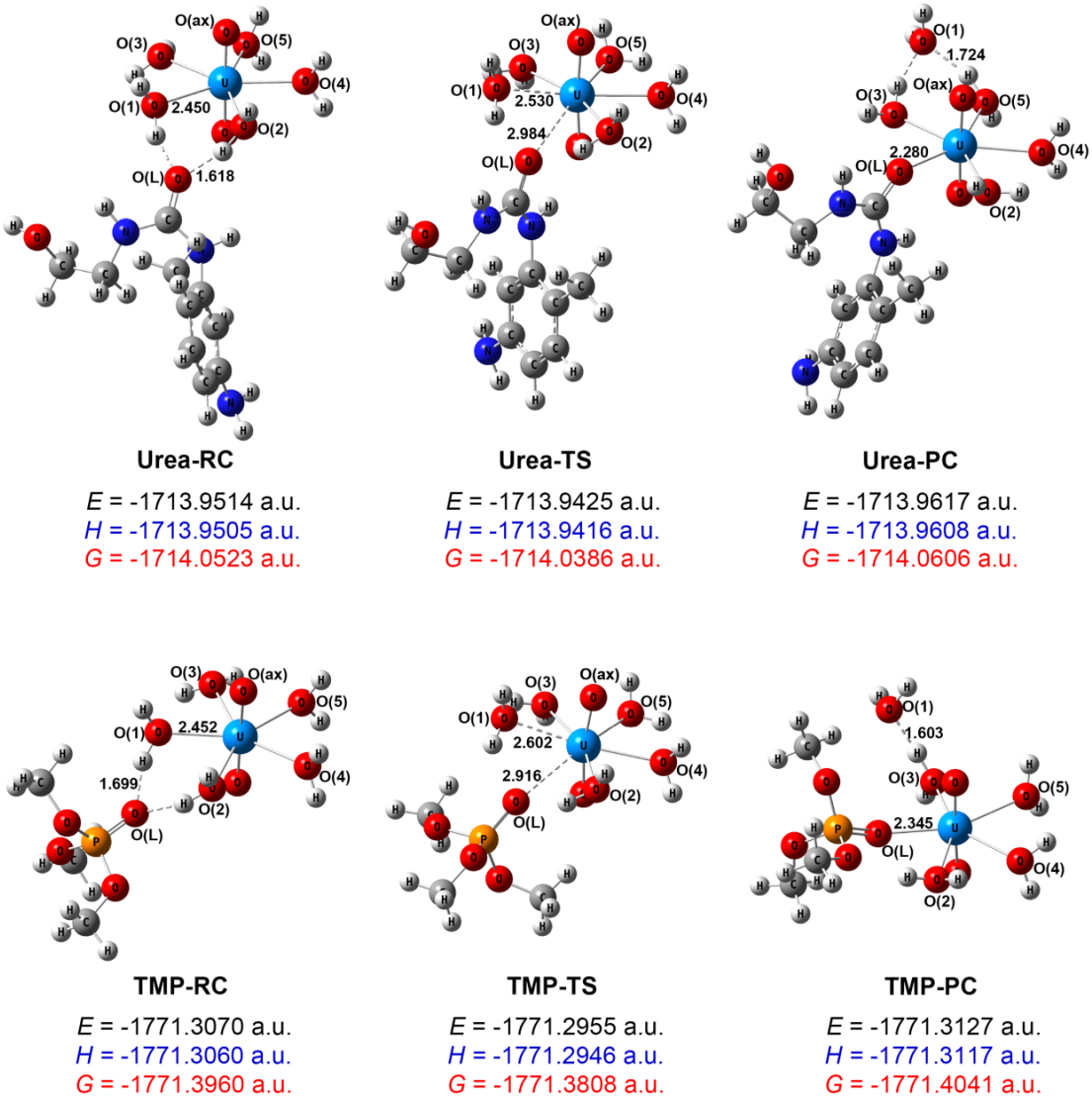


**Figure S7. The optimized structures of reactant complexes (RC), transition states (TS) and product complexes (PC) for urea/TMP extraction processes in aqueous solution (CPCM). The energy and important bond lengths are also shown in this figure.**

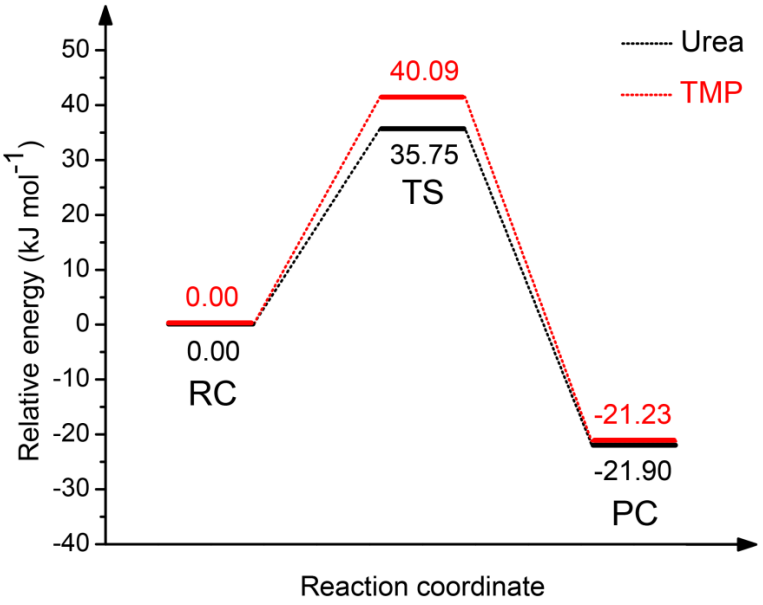


**Figure S8. Relative free energy profiles along uranyl extraction processes of urea and trimethyl phosphate (TMP) in aqueous solution.**

**Table S8. The changes of enthalpy (Δ*H*, kJ mol$^{-1}$), entropy (Δ*S*, J mol$^{-1}$ K$^{-1}$), and gibbs free energy (Δ*G*, kJ mol$^{-1}$) for the interaction between uranyl and the ligand (urea, TMP) in the aqueous solution (CPCM, UFF).**

| | | Δ*H* | Δ*S* | Δ*G* |
|---|---|---|---|---|
| urea | RC→TS | 23.45 | −41.25 | 35.75 |
| | RC→PC | −26.99 | −17.07 | −21.90 |
| TMP | RC→TS | 30.03 | −33.74 | 40.09 |
| | RC→PC | −14.96 | 21.33 | −21.03 |

### 4.2 Natural bond orbital (NBO) analysis

To gain deeper insight into the various bond-breaking or bond-making processes, the Wiberg bond order values (WBOS) were obtained through NBO analysis at the B3LYP/6-31G(d)/RECP level of theory. The percentage of evolution of bond orders (%Ev)[35] is given by

$$(\%\mathrm{Ev})_i = 100 \times [B_i^{\mathrm{TS}} - B_i^{\mathrm{RC}}] / [B_i^{\mathrm{PC}} - B_i^{\mathrm{RC}}] \qquad (1)$$

where $B$ is the bond order and the superscripts TS, RC, and PC refer to the transition state, reactant complex, and product complex, respectively. And also another concept, synchronicity ($S_y$), proposed by Moyano et al.[36] is usually used to describe the global nature of bond breaking/forming process in the reaction and is expressed by

$$S_y = 1 - \frac{\sum_{i=1}^{n} \frac{\left|(\%Ev)_i - (\%Ev)_{av}\right|}{(\%Ev)_{av}}}{2n-2} \qquad (2)$$

In Eq. (2), the average percentage of evolution of bond orders [$(Ev)_{av}$%] is given by

$$(\%Ev)_{av} = \frac{1}{n}\sum_{i=1}^{n}(\%Ev)_i \qquad (3)$$

and $n$ refers to the number of bonds directly involved in the reaction.

The Wiberg bond order values, percentage of evolution of bond orders (%Ev) and synchronicity ($S_y$) in aqueous solution are shown in Table S10 (Table S14 in gas). For the Urea-involving process, the values of WBOs and %Ev combined with the changes in U–O(L) and U–O1($H_2O$) bond lengths (table S9) indicate that the U–O(L) bond-forming (%Ev=33.94%) and U–O1($H_2O$) bond-breaking (%Ev = 10.46%) which corresponds to the process of ligands interchange. We found that the synchronicity values are 0.710 and 0.660 for urea-involving process and TMP-involving process, respectively, which show that the TMP-involving process is almost the same as urea-involving process, and the TMP-process of this mechanism is slightly asynchronous.

**Table S9. The selected geometrical parameters of the reactant complexes (RC), transition states (TS), and product complexes(PC) for extraction reaction processes in the aqueous solution (CPCM, UFF) obtained by the DFT calculations.**

| | | d(U–O1$_{water}$) | d(U–O$_L$) | θ(O$_{water}$–U–O$_L$) | θ(O$_{ax}$–U–O$_{ax}$) |
|---|---|---|---|---|---|
| urea | RC | 2.450 | 3.845 | | 178.51 |
| | TS | 2.530 | 2.984 | 54.71 | 173.27 |
| | PC | 4.113 | 2.280 | | 176.90 |
| TMP | RC | 2.452 | 3.950 | | 179.14 |
| | TS | 2.602 | 2.916 | 57.01 | 170.50 |
| | PC | 4.355 | 2.345 | | 176.89 |

**Table S10. Wiberg bond orders (WBOs), Percentage of Evolution of Bond Orders %$E_v$ and Synchronicity ($S_y$) in the aqueous solution (CPCM, UFF).**

| | | WBOs(RC) | WBOs(TS) | WBOs(PC) | %$E_v$ | $S_y$ |
|---|---|---|---|---|---|---|
| Urea | U—O(L) | 0.014 | 0.215 | 0.686 | 29.92 | |
| | U—O(1) | 0.464 | 0.419 | 0.006 | 9.83 | |
| | U—O(2) | 0.489 | 0.451 | 0.393 | 39.58 | |
| | U—O(3) | 0.402 | 0.421 | 0.433 | 61.29 | 0.710 |
| | U—O(4) | 0.446 | 0.413 | 0.411 | 94.29 | |
| | U—O(5) | 0.420 | 0.413 | 0.464 | −15.91 | |
| TMP | U—O(L) | 0.009 | 0.212 | 0.564 | 36.57 | |
| | U—O(1) | 0.456 | 0.374 | 0.006 | 18.22 | |
| | U—O(2) | 0.477 | 0.439 | 0.414 | 60.32 | |
| | U—O(3) | 0.402 | 0.418 | 0.523 | 13.22 | 0.660 |
| | U—O(4) | 0.447 | 0.419 | 0.391 | 50.00 | |
| | U—O(5) | 0.423 | 0.413 | 0.411 | 83.33 | |

**Table S11. The selected charges and changes in atom charges determined by natural population analysis in the aqueous solution (CPCM, UFF).**

| | | U | O(L) | O(1) | O(2) | O(3) | O(4) | O(5) |
|---|---|---|---|---|---|---|---|---|
| urea | RC | 1.777 | −0.791 | −0.903 | −0.895 | −0.878 | −0.869 | −0.878 |
| | TS | 1.750 | −0.774 | −0.896 | −0.881 | −0.871 | −0.876 | −0.873 |
| | RC→TS | −0.027 | 0.017 | 0.007 | 0.014 | 0.007 | −0.007 | 0.005 |
| | PC | 1.694 | −0.660 | −0.976 | −0.875 | −0.892 | −0.878 | −0.886 |
| TMP | RC | 1.785 | −1.146 | −0.896 | −0.889 | −0.878 | −0.870 | −0.879 |
| | TS | 1.768 | −1.098 | −0.895 | −0.877 | −0.874 | −0.876 | −0.872 |
| | RC→TS | −0.017 | 0.048 | 0.001 | 0.012 | 0.004 | −0.006 | 0.007 |
| | PC | 1.726 | −1.003 | −0.959 | −0.884 | −0.887 | −0.880 | −0.875 |

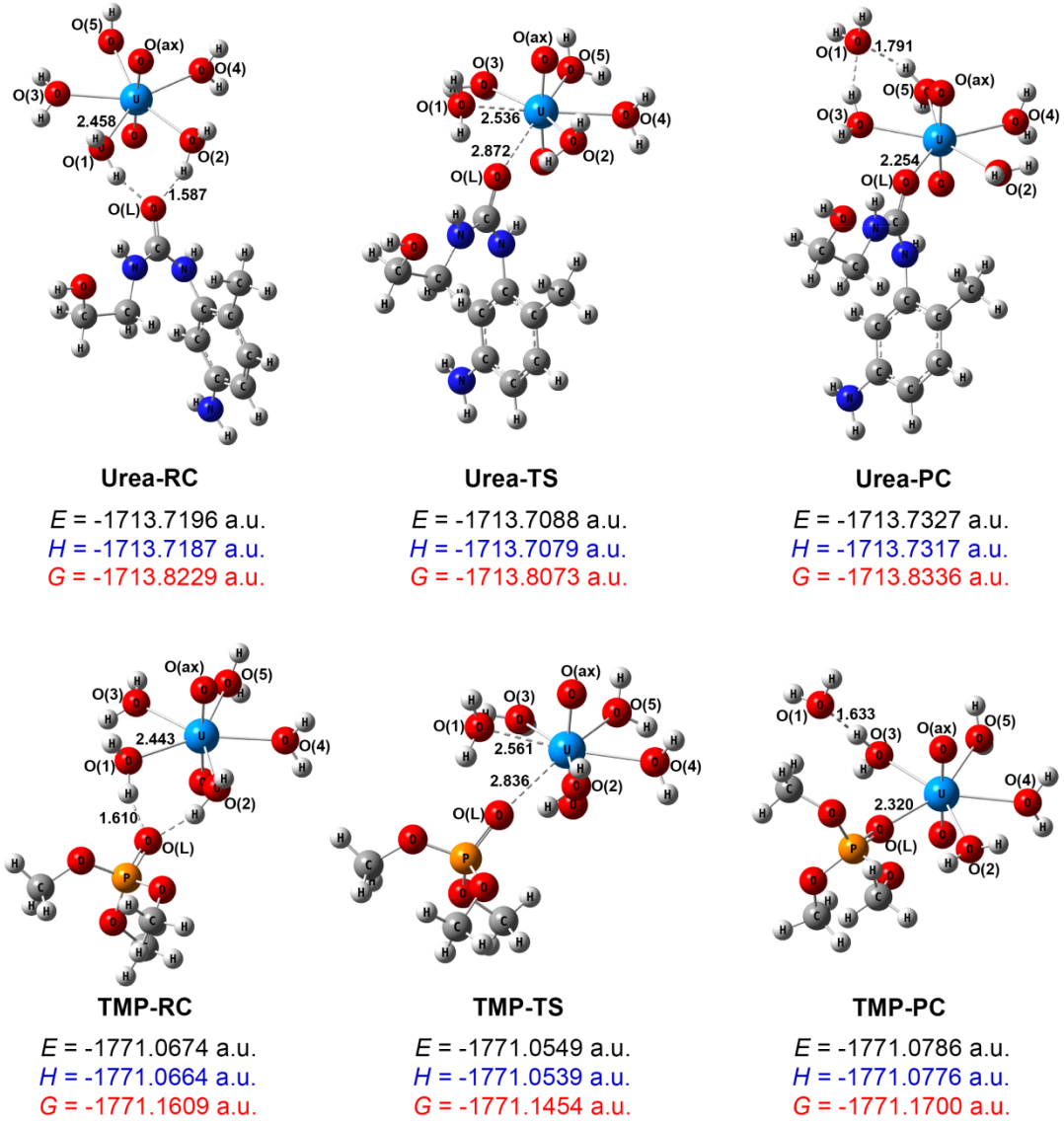


**Figure S9. The optimized structures of reactant complexes (RC), transition states (TS) and product complexes (PC) for urea/TMP extraction processes in gas (298.15 K, 0.1 MPa). The energy and important bond lengths are also shown in this figure.**

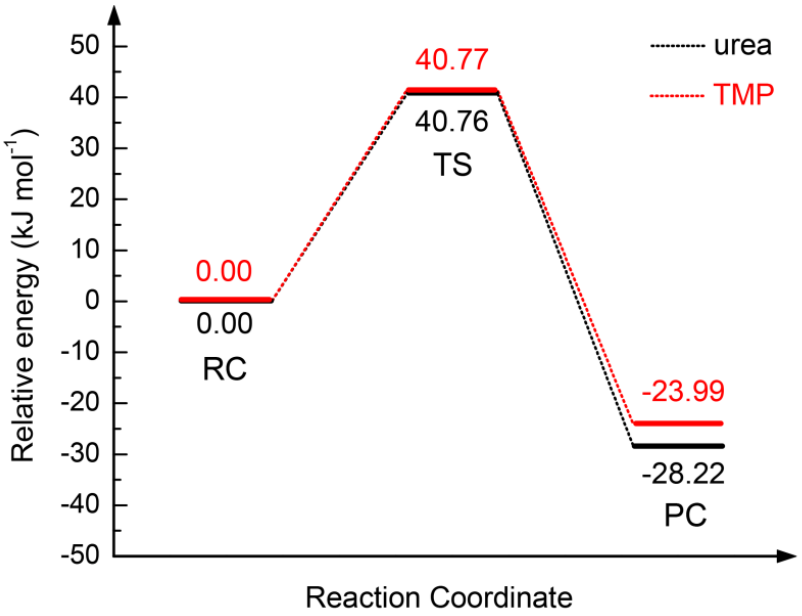


**Figure S10. Relative free energy profiles along uranyl extraction processes of urea and trimethyl phosphate (TMP) in gas (298.15 K, 0.1 MPa).**

**Table S12. The changes of enthalpy (Δ*H*, kJ mol$^{-1}$), entropy (Δ*S*, J mol$^{-1}$ K$^{-1}$), and gibbs free energy (Δ*G*, kJ mol$^{-1}$) for the interaction between uranyl and the ligand (urea, TMP) in gas (298.15 K, 0.1 MPa).**

| | | Δ*H* | Δ*S* | Δ*G* |
|---|---|---|---|---|
| urea | RC→TS | 28.34 | −41.66 | 40.76 |
| | RC→PC | −34.33 | −20.49 | −28.22 |
| TMP | RC→TS | 32.84 | −26.60 | 40.77 |
| | RC→PC | −29.40 | −18.15 | −23.99 |

**Table S13. The selected geometrical parameters of the reactant complexes (RC), transition states (TS), and product complexes (PC) for extraction reaction processes in gas (298.15 K, 0.1 MPa) obtained by the DFT calculations**

| | | d(U–$O_{water}$) | d(U–$O_L$) | θ($O_{water}$–U–$O_L$) | θ($O_{ax}$–U–$O_{ax}$) |
|---|---|---|---|---|---|
| Urea | RC | 2.458 | 3.848 | | 176.75 |
| | TS | 2.536 | 2.872 | 55.55 | 173.07 |
| | PC | 4.146 | 2.254 | | 173.98 |
| TMP | RC | 2.443 | 3.869 | | 176.40 |
| | TS | 2.561 | 2.836 | 57.00 | 169.91 |
| | PC | 4.429 | 2.320 | | 174.04 |

**Table S14. Wiberg bond orders (WBOs), percentage of evolution of bond orders %$E_v$ and synchronicity ($S_y$) in gas (298.15 K, 0.1 MPa).**

| | | WBOs(RC) | WBOs(TS) | WBOs(PC) | %$E_v$ | $S_y$ |
|---|---|---|---|---|---|---|
| Urea | U—O(L) | 0.016 | 0.263 | 0.744 | 33.94 | |
| | U—O(1) | 0.446 | 0.400 | 0.006 | 10.46 | |
| | U—O(2) | 0.462 | 0.422 | 0.371 | 43.96 | |
| | U—O(3) | 0.372 | 0.393 | 0.404 | 65.62 | 0.7178 |
| | U—O(4) | 0.394 | 0.377 | 0.376 | 94.44 | |
| | U—O(5) | 0.375 | 0.382 | 0.428 | 13.21 | |
| TMP | U—O(L) | 0.013 | 0.252 | 0.600 | 40.76 | |
| | U—O(1) | 0.468 | 0.396 | 0.005 | 15.55 | |
| | U—O(2) | 0.492 | 0.443 | 0.412 | 61.25 | |
| | U—O(3) | 0.392 | 0.417 | 0.486 | 26.60 | 0.8305 |
| | U—O(4) | 0.416 | 0.411 | 0.372 | 11.36 | |
| | U—O(5) | 0.398 | 0.406 | 0.389 | −88.89 | |

### 4.3 The effect of nitrate ions on uranium extraction

Similar effect of nitrate ions was also observed in extraction of uranium by TMP in solvent-extraction system (CPCM, UFF) (Table S15). For comparison, the extraction processes are also studied in gas phase (298.15 K, 0.1 MPa). For the reaction $[UO_2(H_2O)_5]^{2+}$ + TMP → $[UO_2(TMP)(H_2O)_4]^{2+}$ + $H_2O$ in aqueous solution, the changes in the Gibbs free energy is −15.55 kJ $mol^{-1}$ (−132.92 kJ $mol^{-1}$ in gas), much more negative than that for the reaction $UO_2(NO_3)_2(H_2O)_2$ + TMP → $[UO_2(NO_3)_2(TMP)(H_2O)_4]$ + $H_2O$ (−2.07 kJ $mol^{-1}$ in aqueous solution and 8.91 kJ $mol^{-1}$ in gas). As shown in Table S16, the WBOs of the U–$O_L$ (Urea and TMP) bonds are larger than those of the U–$O_{water}$ bonds, which indicates that the urea ligands have much stronger coordination ability towards uranyl ions than water molecules.

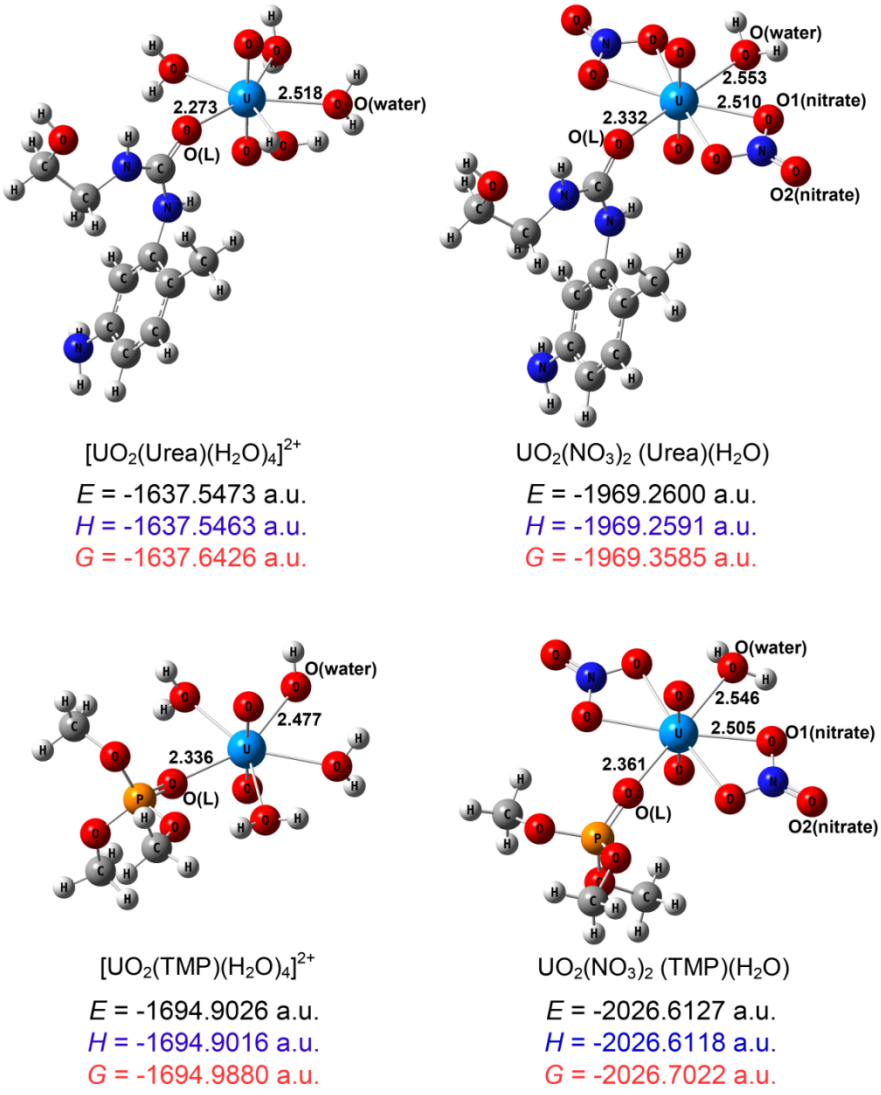


$[UO_2(Urea)(H_2O)_4]^{2+}$

*E* = -1637.5473 a.u.
*H* = -1637.5463 a.u.
*G* = -1637.6426 a.u.

$UO_2(NO_3)_2$ (Urea)($H_2O$)

*E* = -1969.2600 a.u.
*H* = -1969.2591 a.u.
*G* = -1969.3585 a.u.

$[UO_2(TMP)(H_2O)_4]^{2+}$

*E* = -1694.9026 a.u.
*H* = -1694.9016 a.u.
*G* = -1694.9880 a.u.

$UO_2(NO_3)_2$ (TMP)($H_2O$)

*E* = -2026.6127 a.u.
*H* = -2026.6118 a.u.
*G* = -2026.7022 a.u.

**Figure S11. The optimized structures of the stationary points for $[UO_2(Urea)(H_2O)_4]^{2+}$, $UO_2(NO_3)_2(Urea)(H_2O)$, $[UO_2(TMP)(H_2O)_4]^{2+}$ and $UO_2(NO_3)_2(TMP)(H_2O)$ in aqueous solution (CPCM, UFF).**

**Table S15. DFT calculations of the changes in enthalpy (Δ*H*, kJ mol$^{-1}$), entropy (Δ*S*, J mol$^{-1}$ K$^{-1}$), and gibbs free energy (Δ*G*, kJ mol$^{-1}$) for the extraction of uranium in aqueous solution (CPCM, UFF).**

| Extraction reaction | Δ*H* | Δ*S* | Δ*G* |
|---|---|---|---|
| $[UO_2(H_2O)_5]^{2+}$ + Urea → $[UO_2(Urea)(H_2O)_4]^{2+}$ + $H_2O$ | −50.87 | −64.97 | −31.50 |
| $UO_2(NO_3)_2(H_2O)_2$ + Urea → $[UO_2(NO_3)_2(Urea)(H_2O)]$ + $H_2O$ | −35.44 | −42.09 | −22.89 |
| $[UO_2(H_2O)_5]^{2+}$ + TMP → $[UO_2(TMP)(H_2O)_4]^{2+}$ + $H_2O$ | −30.71 | −50.85 | −15.55 |
| $UO_2(NO_3)_2(H_2O)_2$ + TMP → $UO_2(NO_3)_2(TMP)(H_2O)$ + $H_2O$ | −8.40 | −21.23 | −2.07 |

**Table S16. Wiberg bond orders (WBOs) of U–O Bonds and natural charges on the U and O atoms for the complexes of uranyl ion and L (L=TMP and Urea) in aqueous solution (CPCM, UFF).**

| species | U–$O_L$ | U–$O_{water}$ | U–$O1_{nitrate}$ | Q(U) | Q($O_L$) |
|---|---|---|---|---|---|
| $[UO_2(H_2O)_5]^{2+}$ | | 0.433 | | 1.802 | |
| $UO_2(NO_3)_2(H_2O)_2$ | | 0.410 | 0.461 | 1.477 | |
| $[UO_2(Urea)(H_2O)_4]^{2+}$ | 0.699 | 0.416 | | 1.705 | −0.655 |
| $UO_2(NO_3)_2$ (Urea)($H_2O$) | 0.628 | 0.404 | 0.450 | 1.403 | −0.635 |
| $[UO_2(TMP)(H_2O)_4]^{2+}$ | 0.571 | 0.424 | | 1.744 | −1.004 |
| $UO_2(NO_3)_2$(TMP)($H_2O$) | 0.551 | 0.403 | 0.449 | 1.435 | −0.987 |

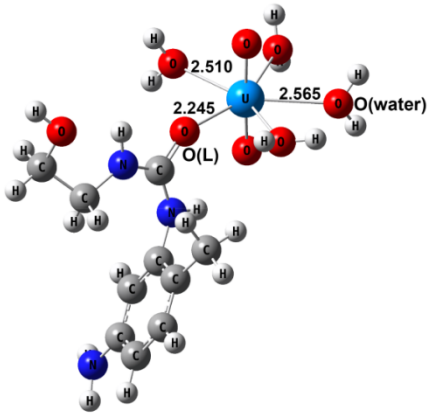


$[UO_2(Urea)(H_2O)_4]^{2+}$

*E* = -1637.3115 a.u.
*H* = -1637.3106 a.u.
*G* = -1637.4091 a.u.

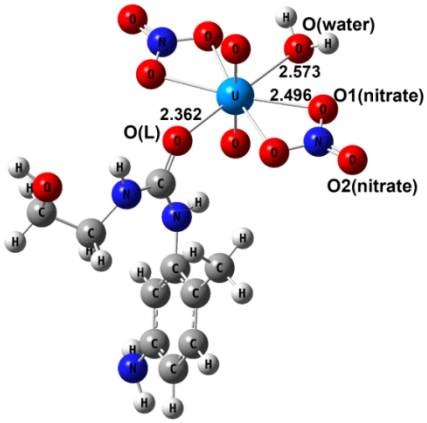


$UO_2(NO_3)_2$ (Urea)($H_2O$)

*E* = -1969.2298 a.u.
*H* = -1969.2288 a.u.
*G* = -1969.3268 a.u.

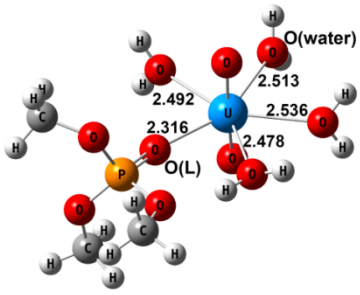


$[UO_2(TMP)(H_2O)_4]^{2+}$

*E* = -1694.6604 a.u.
*H* = -1694.6595 a.u.
*G* = -1694.7475 a.u.

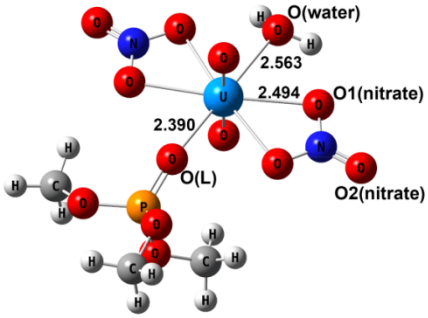


$UO_2(NO_3)_2$ (TMP)($H_2O$)

*E* = -2026.5899 a.u.
*H* = -2026.5890 a.u.
*G* = -2026.6770 a.u.

**Figure S12. The optimized structures of the stationary points for $[UO_2(Urea)(H_2O)_4]^{2+}$, $UO_2(NO_3)_2(Urea)(H_2O)$, $[UO_2(TMP)(H_2O)_4]^{2+}$ and $UO_2(NO_3)_2(TMP)(H_2O)$ in gas (298.15 K, 0.1 MPa).**

**Table S17. DFT calculations of the changes in enthalpy (Δ*H*, kJ mol$^{-1}$), entropy (Δ*S*, J mol$^{-1}$ K$^{-1}$), and gibbs free energy (Δ*G*, kJ mol$^{-1}$) for the extraction of uranium in gas (298.15 K, 0.1 MPa).**

| Extraction reaction | Δ*H* | Δ*S* | Δ*G* |
|---|---|---|---|
| $[UO_2(H_2O)_5]^{2+}$ + Urea → $[UO_2(Urea)(H_2O)_4]^{2+}$ + $H_2O$ | −202.62 | −70.37 | −181.64 |
| $UO_2(NO_3)_2(H_2O)_2$ + Urea → $[UO_2(NO_3)_2$ (Urea)$(H_2O)]$ + $H_2O$ | −41.10 | −48.73 | −26.57 |
| $[UO_2(H_2O)_5]^{2+}$ + TMP → $[UO_2(TMP)(H_2O)_4]^{2+}$ + $H_2O$ | −148.92 | −53.66 | −132.92 |
| $UO_2(NO_3)_2(H_2O)_2$ + TMP → $UO_2(NO_3)_2$ (TMP)$(H_2O)$ + $H_2O$ | −17.01 | −27.17 | −8.91 |

**Table S18. Wiberg bond orders (WBOs) of U–O Bonds and natural charges on the U and O atoms for the complexes of uranyl ion and L (L = TMP and Urea) in gas (298.15 K, 0.1 MPa).**

| species | U–$O_L$ | U–$O_{water}$ | U–$O1_{nitrate}$ | Q(U) | Q($O_L$) |
|---|---|---|---|---|---|
| $[UO_2(H_2O)_5]^{2+}$ | | 0.433 | | 1.802 | |
| $UO_2(NO_3)_2(H_2O)_2$ | | 0.410 | 0.461 | 1.477 | |
| $[UO_2(Urea)(H_2O)_4]^{2+}$ | 0.699 | 0.416 | | 1.705 | −0.655 |
| $UO_2(NO_3)_2$ (Urea)$(H_2O)$ | 0.628 | 0.404 | 0.450 | 1.403 | −0.635 |
| $[UO_2(TMP)(H_2O)_4]^{2+}$ | 0.571 | 0.424 | | 1.744 | −1.004 |
| $UO_2(NO_3)_2(TMP)(H_2O)$ | 0.551 | 0.403 | 0.449 | 1.435 | −0.987 |

# 5. The uranium (VI) extraction experiments.

## 5.1 Effect of pH

The effect of pH on the adsorption capability of Urea-GO toward uranium(VI) was investigated and the results are shown in Fig. S13. The adsorption amount of uranium increased drastically with increasing of pH values.

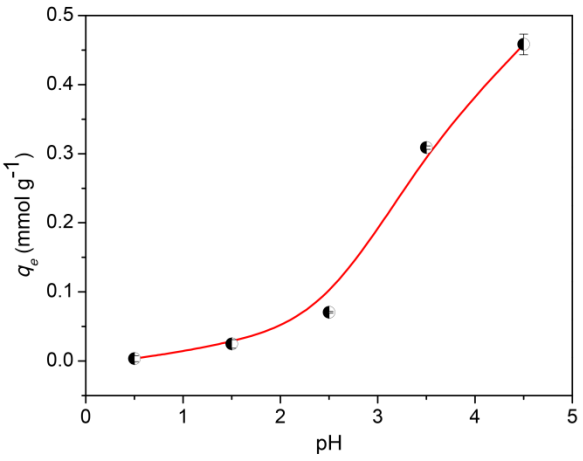

**Figure S13. Effect of pH on the solid-phase extraction of uranyl(VI).** ( the initial concentrations $c_0$ = 0.42 mmol $L^{-1}$ for uranyl ions, the volume of testing solution $V$ = 25 mL, experiment temperatures $T$ = 293 K, all flasks shaking time $t$ = 120 min, and the weight of adsorbent $w$ = 10 mg)

## 5.2 Effect of contact time

The effect of contact time on the uranium(VI) adsorption by Urea-GO was shown in Fig. S14. The adsorption amount of uranyl ions increased rapidly during the first five minutes and then gradually tended to equilibrium. It is worth noting that over 65% of total adsorption amount was achieved in the first minute.

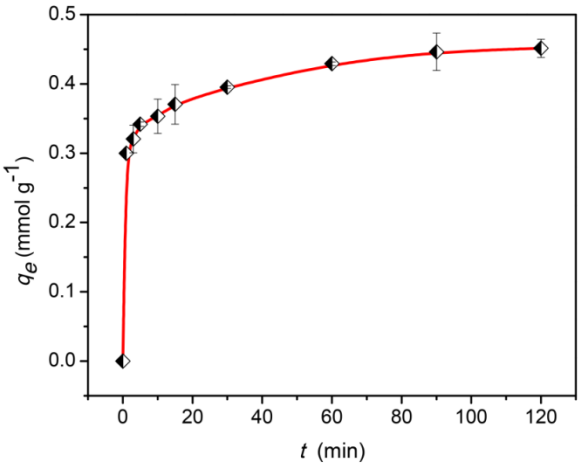


**Figure S14. Effect of contact time on the solid-phase extraction of uranyl(VI).** (pH = 4.5, the initial concentrations $c_0$ = 0.42 mmol $L^{-1}$ for uranyl ions, the volume of testing solution $V$ = 25 mL, experiment temperatures $T$ = 293 K, and the weight of adsorbent $w$ = 10 mg)

## 5.3 Effect of initial concentration

The adsorption isotherm of uranium(VI) were studied by batch equilibrium experiments and the results are presented in Fig. S15. As depicted in Fig. S15, the adsorption amount of uranyl ions by Urea-GO increased with increasing equilibrium U(VI) concentration.

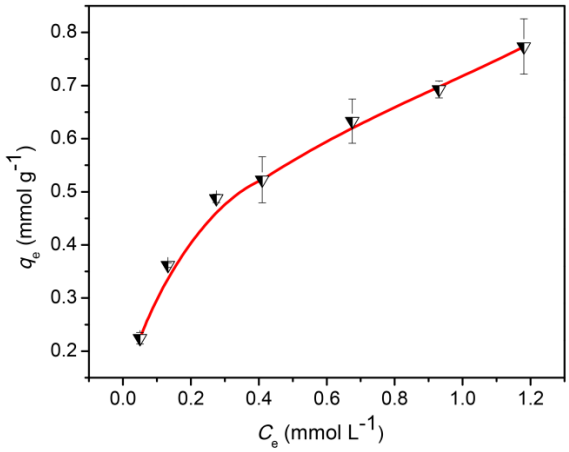


**Figure S15. Effect of initial concentration on the solid-phase extraction of uranyl(VI).** (pH = 4.5, the volume of testing solution $V$ = 25 mL, experiment temperatures $T$ = 293 K, all flasks shaking time $t$ = 120 min and the weight of adsorbent $w$ = 10 mg)

### 5.4 Effect of temperature

The effect of temperature on the adsorption capability of Urea-GO was investigated. As described in Fig. S16, the adsorption amount of uranium(VI) increased with increasing temperature.

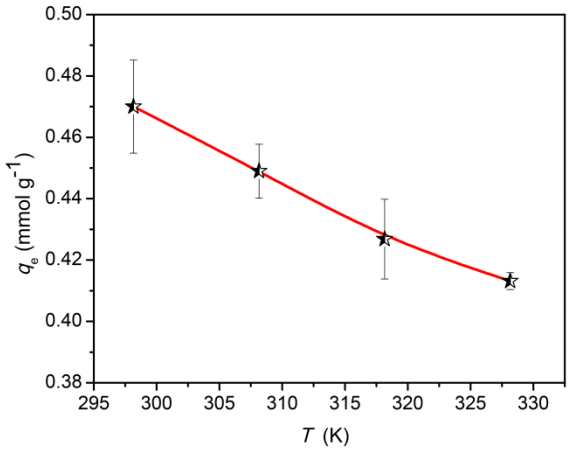


**Figure S16. Effect of temperature on the solid-phase extraction of uranyl(VI).** (pH = 4.5, the initial concentrations $c_0$ = 0.42 mmol L$^{-1}$ for uranyl ions, the volume of testing solution $V$ = 25 mL, and the weight of adsorbent $w$ = 10 mg)

## References

1 W. Hummers and R. Offeman, *J. Am. Chem. Soc.*, 1958, **80**, 1339.

2 S. Stankovich, R. D. Piner, S. T. Nguyen and R. S. Ruoff, *Carbon*, 2006, **44**, 3342.

3 W. Gao, L. B. Alemany, L. Ci and P. M. Ajayan, *Nature Chem.* 2009, **1**, 403

4 D. W. Lee, V. L. De Los Santos, J. W. Seo, L. L. Felix, D. A. Bustamante, J. M. Cole and C. H. W. Barnes, *J. Phys. Chem. B*, 2010, **114**, 5723.

5 C. Xu, X. Wu, J. Zhu and X. Wang, *Carbon*, 2008, **46**, 386.

6 J. H. Saunders and R. J. Slocombe, *Chem. Rev.*, 1948, **43**, 203.

7 S. Park, J. An, R. D. Piner, I. Jung, D. Yang, A. Velamakanni, S. T. Nguyen and R. S. Ruoff, *Chem. Mater.*, 2008, **20**, 6592.

8 C. Shan, H. Yang, J. Song, D. Han, A. Ivaska and L. Niu, *Anal. Chem.*, 2009, **81**, 2378.

9 Y. Yang, J. Wang, J. Zhang, J. Liu, X. Yang and H. Zhao, *Langmuir*, 2009, **25**,11808.

10 X. Ye, R. B. Smith, S. Cui, V. de Almeida and B. Khomami, *Solvent Extr. Ion Exch.*, 2010, **28**, 1.

11 M. Jayasinghe and T. L. Beck, *J. Phys. Chem. B*, 2009, **113**, 11662.

12 J. C. Taylor and M. H. Mueller, Acta Cryst. 1965, **19**, 536.

13 B. N. Dalley, M. H. Mueller and S. H. Simonsen, *Inorg. Chem.*, 1971, **10**, 323.

14 M. Bühl, H. Kabrede, R. Diss and G. Wipff, *J. Am. Chem. Soc.*, 2006, **128**, 6357.

15 G. A. Shamov and G. Schreckenbach, *J. Phys. Chem. A*, 2005, **109**, 10961.

16 C. Wang, J. Lan, Y. Zhao, Z. Chai, Y. Wei and W. Shi, *Inorg. Chem.*, 2013, **52**, 196.

17 K. Sebbari, J. Roques, E. Simoni, C. Domain, H. Perron and H. Catalette, *Surf. Sci.*, 2012, **606**, 1135.

18 S. Tsushima and A. Suzuki, *J. Molec. Struct. (Theochem)*, 2000, **529**, 21.

19 P. Nichols, E. J. Bylaska, G. K. Schenter and W. de Jong, *J. Chem. Phys.*, 2008, **128**, 124507.

20 B. Siboulet, C. J. Marsden and P. Vitorge, *Chem. Phys.*, 2006, **326**, 289.

21 P. J. Hay, R. L. Martin and G. Schreckenbach, *J. Phys. Chem. A*, 2000, **104**, 6259.

22 L. Soderholm, S. Skanthakumar and J. Neuefeind, *Anal. Bioanal. Chem.*, 2005, **383**, 48.

23 L. Sémon, C. Boehme, I. Billard, C. Hennig, K. Lützenkirchen, T. Reich, A. Roßberg, I. Rossini and G. Wipff, *ChemPhysChem*, 2001, **2**, 591.

24 P. G. Allen, J. J. Bucher, D. K. Shuh, N. M. Edelstein and T. Reich, *Inorg. Chem.*, 1997, **36**, 4676.

25 U. Wahlgren, H. Moll, I. Grenthe, B. Schimmelpfennig, L. Maron, V. Vallet and O. Gropen, *J. Phys. Chem. A*, 1999, **103**, 8257

26 M. Åberg, D. Ferri, J. Glaser and I. Grenthe, *Inorg. Chem.*, 1983, **22**, 3986.

27 J. Neuefeind, L. Soderholm and S. Skanthakumar, *J. Phys. Chem. A*, 2004, **108**, 2733.

28 C. Den Auwer, R. Drot, E. Simoni, S. D. Conradson, M. Gailhanou and J. Mustre de Leon, *New J. Chem.*, 2003, **27**, 648.

29 J. S. Craw, M. A. Vincent, I. H. Hiller and A. L. Wallwork, *J. Phys. Chem.*, 1995, **99**, 10181.

30 I. A. Charushnikova and C. Den Auwer, *Russ. J. Coord. Chem.*, 2004, **30**, 511.

31 K. L. Nash, R. E. Barrans, R. Chiarizia, M. L. Dietz, M. P. Jensen and P. G. Rickert, *Solvent Extr. Ion Exch.*, 2000, **18**, 605.

32 X. Ye, S. Cui, V. F. de Almeida and B. Khomami, *J. Phys. Chem. B*, 2009, **113**, 9852.

33 X. Ye, S. Cui, V. F. de Almeida, B. P. Hay and B. Khomami, *Phys. Chem. Chem. Phys.*, 2010, **12**, 15406.

34 X. Sun, X. Wei, X. Wu, Y. Ren, N. Wong, W. Li, *J. Phys. Chem. A*, 2010, **114**, 595.

35 J. Gao, Y. Zeng, C. Zhang, Y. Xue, *J. Phys. Chem. A*, 2009, **113**, 325.

36 A. Moyano, M. A. Pericàs, A. Valenti, *J. Org. Chem.*, 1989, **54**, 573.